RSC Advances

PAPER

View Article Online
View Journal | View Issue

Cite this: *RSC Adv.*, 2020, **10**, 44768

The importance of Asn52 in the structure–function relationship of human cytochrome *c*†

Dan Lou,‡[a] Xi-Chun Liu,‡[a] Xiao-Juan Wang,[a] Shu-Qin Gao,[b] Ge-Bo Wen[b] and Ying-Wu Lin *[ab]

Received 24th November 2020
Accepted 7th December 2020

DOI: 10.1039/d0ra09961a

rsc.li/rsc-advances

The function of the highly conserved residue Asn52 in human cytochrome *c* (H-Cyt *c*) is not fully understood. Herein, we show that the naturally occurring variant N52S H-Cyt *c* has a perturbed secondary structure, with a small fraction of high-spin species. Remarkably, it exhibits an enhanced peroxidase activity by 3–8-fold at neutral pH, as well as self-oxidation in reaction with H_2O_2. This study suggests that the H-bond network mediated by Asn52 is essential to suppress the apoptotic activity of H-Cyt *c* under physiological conditions.

Cytochrome *c* (Cyt *c*) is an important member of a widely distributed group of redox metalloproteins.[1–4] Human mitochondrial cytochrome *c* (H-Cyt *c*) is a small heme protein (104 residues) with a covalently attached heme group *via* two thioester bonds. The central iron is coordinated by His18 on the proximal side and Met80 on the distal side. The main function of H-Cyt *c* is to transfer electrons between Cyt *c* and Cyt *c* oxidase in the respiratory chain.[5] In addition to playing an indispensable role in substance metabolism and energy conversion, Cyt *c* is engaged in an early stage of the intrinsic apoptosis pathway.[6,7] Cyt *c* exhibits peroxidase activity when it interacts with the lipid cardiolipin (CL) in the mitochondrial inner membrane, resulting in the oxygenation of CL and the release of Cyt *c* into the cytoplasm, which subsequently induces the formation of the apoptosome complex and ultimately leads to cell death.[8,9]

The obtain peroxidase activity, Cyt *c* undergoes a conformational change. Typically, the distal ligand Met80 dissociates from the hexa-coordinated heme iron while the proximal ligand His18 is essential to maintain protein structure. A large number of studies have shown that perturbation of the heme pocket can modulate the stability and activity by mutating the key residues in Cyt *c*.[10] The peroxidase activity of Cyt *c* can be enhanced under alkaline condition by conformational change called "alkaline transition" with a typical pK_a between 9 and 9.5.[4,11] Protein crystallography studies show a hydroxide or the N_ε atom of Lys73/79 residue in the Ω loop 70–85 can replace the distal Met80 ligand of the ferric Cyt *c*.[12,13] In recent years, it has been discovered that alkaline transition can occur at physiological pH with certain post-translation modifications in Cyt *c*, such as Tyr74 nitration and Tyr48 phosphorylation.[14–16] Bowler and co-workers also reported that when Cyt *c* interacts with detergents, it loses Met80 ligation and forms a well-defined pocket for binding of hydrocarbons, which is a structural mimic for Cyt *c* mediated cardiolipin oxidation.[17] These conformers with enhanced peroxidase activity are useful models for studying the conformational change of Cyt *c* on the onset of instinct apoptotic process.

Up to date, four pathogenic mutations (G41S,[18] Y48H,[19] A51V,[20] and Lys100del[21]) have been reported to associate with a low platelet count disease, an autosomal dominant thrombocytopenia 4 (THC4). Three of the four variants are located on the Ω loop 40–57 and show enhanced peroxidase activity.[22–27] In 2016, a massive sequencing study identified a N52S mutation in the H-Cyt *c*.[4,28] Although the disease-relevance of the N52S missense mutation is still unclear, the Asn52 residue is one of most conserved residues in eukaryotic Cyt *c*, as revealed by sequence alignment and structure analysis.[10,29] Protein crystallography studies showed that Asn52 forms H-bonds with heme propionate-7 and a structural water molecule, which further interacts with Tyr67 and Thr78 in the ferric state (Fig. 1).[30,31] Recent NMR characterization revealed that Asn52 also forms dynamic H-bond with heme propionate-6 in the ferrous state.[32] These observations indicate that Asn52 is critical for protein stability, folding and the crosstalk between the Ω loops 40–57 and 70–85. In addition, Asn52 is proposed to interact with CL and involved in the formation of the hydrocarbon binding pocket.[33–35] Moreover, the studies of the iso-1-cytochrome *c* suggest Asn52 mutation affects the electron transfer.[36]

In the present study, we constructed both N52S and N52A variants to ascertain the importance of highly conserved residue Asn52 in H-Cyt *c*. The protein was expressed in the *E. coli* BL21(DE3) stain and the purified protein was certificated by electrospray ionization mass spectrometer (ESI-MS). It showed

[a]*School of Chemistry and Chemical Engineering, University of South China, Hengyang 421001, China. E-mail: ywlin@usc.edu.cn*

[b]*Laboratory of Protein Structure and Function, University of South China Medical School, Hengyang 421001, China*

† Electronic supplementary information (ESI) available: Experimental details, UV-Vis, mass spectra and kinetic studies. See DOI: 10.1039/d0ra09961a

‡ These authors contributed equally.

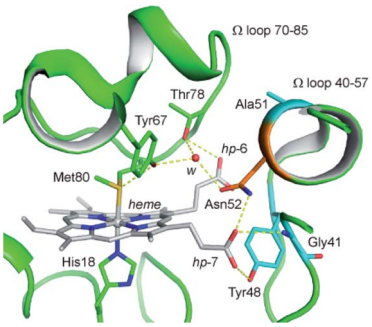

Fig. 1 Close up view of the H-bond networks around Asn52 and the heme crevice in the ferric WT H-Cyt *c* (PDB code 3ZCF[31]). Asn52 was shown as orange stick. The heme iron and heme cofactor were shown as grey ball and sticks, respectively. H-bonds were shown as yellow dash lines. A structural water molecule (*w*) was shown as red sphere. The heme propionates 6 and 7 were referred to as *hp*-6 and *hp*-7. The residues Gly41, Tyr48, and Ala51 linked to the disease THC4 were shown as cyan sticks.

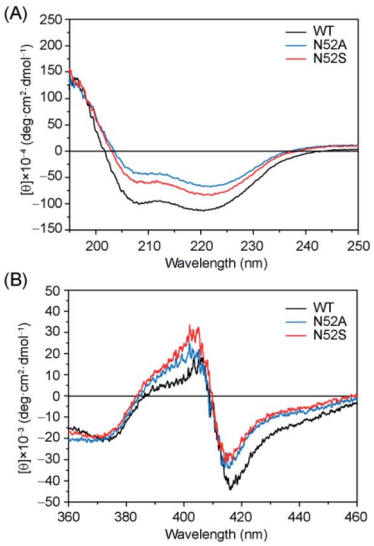

Fig. 2 Comparison of the CD spectra in the (A) far-UV region and (B) visible region. Spectra were colored as black, blue, and red for the ferric WT, N52A, and N52S H-Cyt *c*, respectively.

a molecular weight of 12 207.0 Da and 12 191.0 Da for the ferric N52S and N52A H-Cyt *c*, respectively, which is in agreement with the calculated mass (N52S, 12 206.9 Da, and N52A, 12 190.9 Da, Fig. S1†). The UV-Vis spectra of both Ser52 and Ala52 variants are highly similar with that of the wild-type (WT) H-Cyt *c* (Fig. S2†). The absorptions at 415, 521 and 550 nm in ferrous state increased slightly in intensity compared to those of WT H-Cyt *c*. These spectral features indicate that the first coordination sphere of the heme iron is roughly preserved in the N52S and N52A variants at pH 7.0, where Met80 still persists as a distal ligand.

In order to investigate whether there were any secondary structure changes induced by the Asn-to-Ser/Ala substitution in position 52, we performed circular dichroism (CD) spectroscopy studies. The far-UV CD spectra of N52S, N52A, and WT H-Cyt *c* all showed a characteristic α-helical structure with a positive peak at 190 nm and broad negative peaks at 208 nm and 222 nm (Fig. 2A). Meanwhile, the ellipticity (θ) value from 200 to 240 nm increased for the N52S and N52A variants, which suggests that the protein might loss some of the α-helical structure as a result of Asn-to-Ser/Ala substitution, likely due to local conformational changes. Moreover, the CD spectra in the Soret band region changed as well (Fig. 2B). The N52S and N52A variants showed a stronger positive peak at 404 nm and a weaker negative peak at 418 nm compared to those of WT H-Cyt *c*. These data show that the Ser/Ala substitution in position 52 alters the geometry/strength of the heme coordination state, as well as the local micro-environment, which is presumably due to the perturbation of the H-bond network mediated by Asn52.

To further reveal the heme micro-environment as a result of conformational changes in the N52S and N52A variants, we performed electron paramagnetic resonance (EPR) studies. The spin states of the ferric heme iron were monitored at 20 K (Fig. 3). Control experiment showed that WT H-Cyt *c* was totally in a low-spin state ($g_z = 3.09$, $g_y = 2.17$) at neutral pH due to the coordination of Met80/His18. The N52A variant was also primarily in a low-spin state with typical EPR signals ($g_z = 3.06$ and $g_y = 2.20$). In contrast to WT and N52A H-Cyt *c*, a small fraction of high-spin species ($g_\perp = 5.95$) was observed in EPR spectra for N52S H-Cyt *c*, which is similar to those observed for other heme proteins, such as myoglobin and neuroglobin variants.[37–39] Note that this characteristic could not be detected using UV-Vis spectroscopy. Instead, the EPR technology revealed a small fraction of N52S H-Cyt *c* in high-spin state, which is likely due to the dissociation of Met80 from the heme iron as a result of structural perturbation by the N52S mutation.

As aforementioned, high-spin species of Cyt *c* typically exhibits peroxidase activity. According to EPR observation, the N52S H-Cyt *c* might exhibit an enhanced peroxidase activity compared to the WT and N52A H-Cyt *c*. To confirm this speculation, we performed a series of kinetic studies to measure the peroxidase activity. First, the reaction with hydrogen peroxide was carried out, in the absence of substrates H-Cyt *c* catalyzes

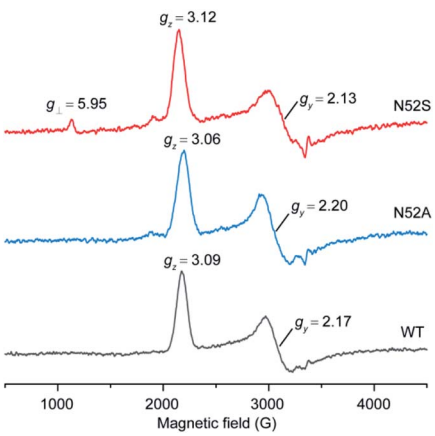

Fig. 3 EPR spectra of ferric WT (black), N52A (blue), and N52S (red) H-Cyt *c* (0.25 mM), collected at 20 K, 2 mW power and 9.4 GHz.

the oxidation of itself, resulting in heme degradation, as indicated by the decrease of the Soret band over time (Fig. 4A and S3†). The heme degradation rates (k_{obs}) were obtained at various the concentrations of H_2O_2. The rate constants were calculated to be 0.52 ± 0.01 M^{-1} s^{-1} for N52S variant and 0.34 ± 0.01 M^{-1} s^{-1} for N52A variant, respectively, by linear fitting of the data (Fig. 4B), which is ~6 times and ~4 times faster than that of WT H-Cyt *c* (0.08 ± 0.01 M^{-1} s^{-1}). Moreover, the self-oxidation of N52S H-Cyt *c* was monitored by using mass spectrometry (Fig. 4C).[40] The mass spectrum of N52S variant showed that a series of oxidized products (+16 and +32 Da) were formed with incubation of H_2O_2 (0.1 mM) for 10 minutes, which was more obvious than those for N52A and WT H-Cyt *c* (Fig. S4†). These observations indicate that the N52S variant is more sensitive to H_2O_2, even with a low concentration.

In addition to the heme degradation assay, we measured the peroxidase activities of H-Cyt *c* using guaiacol and 2,2′-azinobis-3-ethylbenzthiazoline-6-sulphonate (ABTS) as typical substrates and H_2O_2 as an oxidant (Fig. 5A and B). The optimal concentration of H_2O_2 was found to be 200 mM and 100 mM for guaiacol and ABTS, respectively, based on the catalysis reaction at varies concentrations of H_2O_2 (Fig. S5†). With the optimal concentration of H_2O_2, the catalytic reactions at different substrate concentrations were performed (Fig. S6 and S7†), and the kinetic parameters were obtained by fitting data to the Mickaelis–Menten equation. As shown in Table 1, the K_m values were not largely affected by the N52A and N52S mutations. Meanwhile, these mutations lead to a significant increase in catalytic rate. The k_{cat} values of N52S and N52A variants for guaiacol oxidation are ~8-fold and ~6-fold higher than that of WT H-Cyt *c*, respectively. For ABTS oxidation, the k_{cat} values of N52S and N52A variants are ~3-fold and ~2-fold higher than that of WT H-Cyt *c*, respectively.

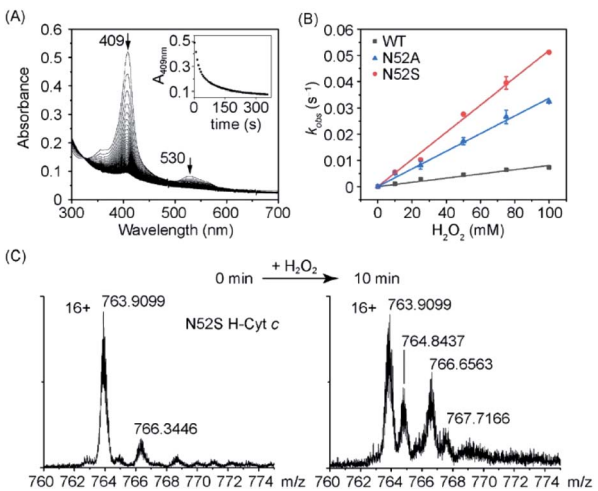

Fig. 4 Heme degradation of H-Cyt *c* in reaction with H_2O_2. (A) Time-dependent UV-Vis spectra of N52S H-Cyt *c*. The absorptions of the Soret band (409 nm) were recorded to calculate the k_{obs}. (B) Linear fitting of k_{obs} as a function of H_2O_2 concentrations. (C) Mass spectra of N52S H-Cyt *c* acquired before and after incubation with H_2O_2 (0.1 mM) for 10 min, and the fragments with a maximum intensity (16+ charges) were shown for clarification.

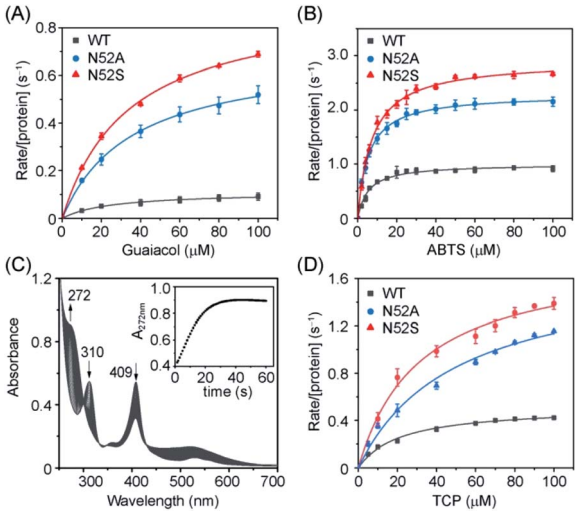

Fig. 5 Steady-state rates of oxidation as a function of guaiacol (A), ABTS (B) and TCP (D) concentration catalyzed by WT (black), N52A (blue), and N52S (red) H-Cyt *c*. (C) UV-Vis spectra of TCP (0.1 mM) dehalogenation catalyzed by N52S H-Cyt *c* (C, 5 μM) in presence of H_2O_2 (20 mM). The experiments were carried out in triplicate and the data were fitted to the Michaelis–Menten equation.

Moreover, we determined the dehaloperoxidase activity using 2,4,6-trichlorophenol (TCP) as a typical substrate. As shown in Fig. 5C, N52S H-Cyt *c* was able to catalyze the dehalogenation of TCP. Upon addition of H_2O_2, the absorbance of TCP at 310 nm decreased rapidly and a characteristic absorption peak (272 nm) of 2,6-dichloroquinone (DCQ) was produced. Steady-state kinetic studies further showed that in dehalogenation of TCP, the k_{cat} values of N52S and N52A H-Cyt *c* were similar, with both ~3-fold higher than that of WT H-Cyt *c* (Table 1). These results thus confirm that the N52S and N52A variants exhibit enhanced peroxidase activities.

It should be noted that there did not seem to be strong correlation between the catalytic properties and the high-spin population of Cyt *c*, since although only N52S Cyt *c* showed a small population of high-spin species in EPR spectroscopy

Table 1 Kinetic parameters for H_2O_2-dependent oxidation of guaiacol, ABTS, and TCP catalyzed by WT, N52A, and N52S H-Cyt *c*

Protein	k_{cat} (s^{-1})	K_m (μM)	k_{cat}/K_m (M^{-1} s^{-1})
	Guaiacol		
WT Cyt *c*	0.11 ± 0.1	24.94 ± 2.13	4400
N52A Cyt *c*	0.7 ± 0.1	35.87 ± 1.64	19 500
N52S Cyt *c*	0.92 ± 0.2	34.22 ± 1.74	26 900
	ABTS		
WT Cyt *c*	1.00 ± 0.02	5.38 ± 0.53	185 900
N52A Cyt *c*	2.29 ± 0.02	5.30 ± 0.21	432 100
N52S Cyt *c*	2.92 ± 0.03	7.34 ± 0.32	397 800
	2,4,6-TCP		
WT Cyt *c*	0.52 ± 0.02	21.52 ± 2.21	24 200
N52A Cyt *c*	1.70 ± 0.12	49.88 ± 7.97	34 100
N52S Cyt *c*	1.8 ± 0.08	31.58 ± 4.05	57 000

(Fig. 3), rate-enhancements were also observed for N52A Cyt *c* (Table 1). To further provide evidence for the lability of Met80, we performed kinetic studies of azide binding.[24] As shown in Fig. S8,† the observed rate constants were calculated to $8.4 \pm 1.5 \times 10^{-3}$ s^{-1} and $4.8 \pm 0.6 \times 10^{-3}$ s^{-1} for N52S and N52A variants, respectively, which is 2–3-fold higher than that of WT H-Cyt *c* ($2.6 \pm 0.9 \times 10^{-3}$ s^{-1}), indicating the weakness of Met80 binding in both variants, especially for N52S Cyt *c*.

In conclusion, our study on the naturally occurring N52S variant of H-Cyt *c* provided valuable insight into the structure–function of the highly conserved residue of Asn52. The mutation of Asn to Ser in position 52 enhanced the peroxidase activity of H-Cyt *c* by 3–8-fold, depending on the substrates, which was comparable to those disease-relevant mutations (G41S, Y48H, and A51V) located on the Ω loop 40–57.[27] In particular, a high-spin species was detected for N52S H-Cyt *c* variant at neutral pH by EPR studies. Structural perturbation of the Ω loops 40–57 and 70–85 might weak the coordination bond of Fe(III)-Met80 and subsequently promote the formation of the high-spin species. Therefore, this study suggests that a conserved proper residue of Asn in position 52 is essential to suppress the peroxidase activity of H-Cyt *c*.

Conflicts of interest

There are no conflicts to declare.

Acknowledgements

This work was supported by the National Natural Science Foundation of China (No. 21977042). EPR spectra were collected on the steady high magnetic field facilities, high magnetic field laboratory (Hefei, China).

References

1 I. Bertini, G. Cavallaro and A. Rosato, *Chem. Rev.*, 2006, **106**, 90–115.
2 L. J. Smith, A. Kahraman and J. M. Thornton, *Proteins*, 2010, **78**, 2349–2368.
3 J. Liu, S. Chakraborty, P. Hosseinzadeh, Y. Yu, S. L. Tian, I. Petrik, A. Bhagi and Y. Lu, *Chem. Rev.*, 2014, **114**, 4366–4469.
4 D. Alvarez-Paggi, L. Hannibal, M. A. Castro, S. Oviedo-Rouco, V. Demicheli, V. Tortora, F. Tomasina, R. Radi and D. H. Murgida, *Chem. Rev.*, 2017, **117**, 13382–13460.
5 S. Yoshikawa and A. Shimada, *Chem. Rev.*, 2015, **115**, 1936–1989.
6 Y. L. P. Ow, D. R. Green, Z. Hao and T. W. Mak, *Nat. Rev. Mol. Cell Biol.*, 2008, **9**, 532–542.
7 A. V. Kulikov, E. S. Shilov, I. A. Mufazalov, V. Gogvadze, S. A. Nedospasov and B. Zhivotovsky, *Cell. Mol. Life Sci.*, 2012, **69**, 1787–1797.
8 V. E. Kagan, V. A. Tyurin, J. Jiang, Y. Y. Tyurina, V. B. Ritov, A. A. Amoscato, A. N. Osipov, N. A. Belikova, A. A. Kapralov, V. Kini, I. I. Vlasova, Q. Zhao, M. Zou, P. Di, D. A. Svistunenko, I. V. Kurnikov and G. G. Borisenko, *Nat. Chem. Biol.*, 2005, **1**, 223–232.
9 P. P. Parui, Y. Sarakar, R. Majumder, S. Das, H. Yang, K. Yasuhara and S. Hirota, *Chem. Sci.*, 2019, **10**, 9140–9151.
10 S. Zaidi, M. I. Hassan, A. Islam and F. Ahmad, *Cell. Mol. Life Sci.*, 2014, **71**, 229–255.
11 H. Theorell and Å. Åkesson, *J. Am. Chem. Soc.*, 1941, **63**, 1818–1820.
12 L. J. McClelland, T. C. Mou, M. E. Jeakins-Cooley, S. R. Sprang and B. E. Bowler, *Proc. Natl. Acad. Sci. U. S. A.*, 2014, **111**, 6648–6653.
13 J. F. Amacher, F. F. Zhong, G. P. Lisi, M. Q. Zhu, S. L. Alden, K. R. Hoke, D. R. Madden and E. V. Pletneva, *J. Am. Chem. Soc.*, 2015, **137**, 8435–8449.
14 J. M. Garcia-Heredia, I. Diaz-Moreno, P. M. Nieto, M. Orzaez, S. Kocanis, M. Teixeira, E. Perez-Paya, A. Diaz-Quintana and M. A. De la Rosa, *Biochim. Biophys. Acta, Bioenerg.*, 2010, **1797**, 981–993.
15 I. Diaz-Moreno, J. M. Garcia-Heredia, A. Diaz-Quintana, M. Teixeira and M. A. De la Rosa, *Biochim. Biophys. Acta, Bioenerg.*, 2011, **1807**, 1616–1623.
16 J. M. Garcia-Heredia, I. Diaz-Moreno, A. Diaz-Quintana, M. Orzaez, J. A. Navarro, M. Hervas and M. A. De la Rosa, *FEBS Lett.*, 2012, **586**, 154–158.
17 L. J. McClelland, H. B. Steele, F. G. Whitby, T. C. Mou, D. Holley, J. B. Ross, S. R. Sprang and B. E. Bowler, *J. Am. Chem. Soc.*, 2016, **138**, 16770–16778.
18 I. M. Morison, E. M. Cramer Borde, E. J. Cheesman, P. L. Cheong, A. J. Holyoake, S. Fichelson, R. J. Weeks, A. Lo, S. M. K. Davies, S. M. Wilbanks, R. D. Fagerlund, M. W. Ludgate, F. Tatley, M. S. A. Coker, N. A. Bockett, G. Hughes, D. A. Pippig, M. P. Smith, C. Capron and E. C. Ledgerwood, *Nat. Genet.*, 2008, **40**, 387–389.
19 D. De Rocco, C. Cerqua, P. Goffrini, G. Russo, A. Pastore, F. Meloni, E. Nicchia, C. T. Moraes, A. Pecci, L. Salviati and A. Savoia, *Biochim. Biophys. Acta, Mol. Basis Dis.*, 2014, **1842**, 269–274.
20 L. Ong, I. M. Morison and E. C. Ledgerwood, *Br. J. Haematol.*, 2017, **176**, 268–279.
21 Y. Uchiyama, K. Yanagisawa, S. Kunishima, M. Shiina, Y. Ogawa, M. Nakashima, J. Hirato, E. Imagawa, A. Fujita, K. Hamanaka, S. Miyatake, S. Mitsuhashi, A. Takata, N. Miyake, K. Ogata, H. Handa, N. Matsumoto and T. Mizuguchi, *Clin. Genet.*, 2018, **94**, 548–553.
22 T. M. Josephs, M. D. Liptak, G. Hughes, A. Lo, R. M. Smith, S. M. Wilbanks, K. L. Bren and E. C. Ledgerwood, *J. Biol. Inorg Chem.*, 2013, **18**, 289–297.
23 A. I. Karsisiotis, O. M. Deacon, M. T. Wilson, C. Macdonald, T. M. A. Blumenschein, G. R. Moore and J. A. R. Worrall, *Sci. Rep.*, 2016, **6**, 30447.
24 O. M. Deacon, A. I. Karsisiotis, T. Moreno-Chicano, M. A. Hough, C. Macdonald, T. M. A. Blumenschein, M. T. Wilson, G. R. Moore and J. A. R. Worrall, *Biochemistry*, 2017, **56**, 6111–6124.
25 M. D. Liptak, R. D. Fagerlund, E. C. Ledgerwood, S. M. Wilbanks and K. L. Bren, *J. Am. Chem. Soc.*, 2011, **133**, 1153–1155.

26 H. Lei and B. E. Bowler, *J. Phys. Chem. B*, 2019, **123**, 8939–8953.
27 O. M. Deacon, R. W. White, G. R. Moore, M. T. Wilson and J. A. R. Worrall, *J. Inorg. Biochem.*, 2020, **203**, 110924.
28 M. Lek, K. J. Karczewski, E. V. Minikel, K. E. Samocha, E. Banks, T. Fennell, A. H. O'Donnell-Luria, J. S. Ware, A. J. Hill, B. B. Cummings, T. Tukiainen, D. P. Birnbaum, J. A. Kosmicki, L. E. Duncan, K. Estrada, F. M. Zhao, J. Zou, E. Pierce-Hollman, J. Berghout, D. N. Cooper, N. Deflaux, M. DePristo, R. Do, J. Flannick, M. Fromer, L. Gauthier, J. Goldstein, N. Gupta, D. Howrigan, A. Kiezun, M. I. Kurki, A. L. Moonshine, P. Natarajan, L. Orozeo, G. M. Peloso, R. Poplin, M. A. Rivas, V. Ruano-Rubio, S. A. Rose, D. M. Ruderfer, K. Shakir, P. D. Stenson, C. Stevens, B. P. Thomas, G. Tiao, M. T. Tusie-Luna, B. Weisburd, H. H. Won, D. M. Yu, D. M. Altshuler, D. Ardissino, M. Boehnke, J. Danesh, S. Donnelly, R. Elosua, J. C. Florez, S. B. Gabriel, G. Getz, S. J. Glatt, C. M. Hultman, S. Kathiresan, M. Laakso, S. NcCarroll, M. I. McCarthy, D. McGovern, R. McPherson, B. M. Neale, A. Palotie, S. M. Purcell, D. Saleheen, J. M. Scharf, P. Sklar, P. F. Sullivan, J. Tuomilehto, M. T. Tsuang, H. C. Watkins, J. G. Wilson, M. J. Daly, D. G. MacArthur and C. Exome Aggregation, *Nature*, 2016, **536**, 285–291.
29 L. Banci, I. Bertini, A. Rosato and G. Varani, *J. Biol. Inorg Chem.*, 1999, **4**, 824–837.
30 C. M. Lett, A. M. Berghuis, H. E. Frey, J. R. Lepock and J. G. Guillemette, *J. Biol. Chem.*, 1996, **271**, 29088–29093.
31 B. S. Rajagopal, A. N. Edzuma, M. A. Hough, K. L. I. M. Blundell, V. E. Kagan, A. A. Kapralov, L. A. Fraser, J. N. Butt, G. G. Silkstone, M. T. Wilson, D. A. Svistunenko and J. A. R. Worrall, *Biochem. J.*, 2013, **456**, 441–452.
32 M. Imai, T. Saio, H. Kumeta, T. Uchida, F. Inagaki and K. Ishimori, *Biochem. Biophys. Res. Commun.*, 2016, **469**, 978–984.
33 M. Rytomaa and P. K. Kinnunen, *J. Biol. Chem.*, 1994, **269**, 1770–1774.
34 Y. L. Deng, F. F. Zhong, S. L. Alden, K. R. Hoke and E. V. Pletneva, *Biochemistry*, 2018, **57**, 5827–5840.
35 Y. L. Deng, M. L. Weaver, K. R. Hoke and E. V. Pletneva, *Inorg. Chem.*, 2019, **58**, 14085–14106.
36 T. B. Karpishin, M. W. Grinstaff, S. Komar-Panicucci, G. McLendon and H. B. Gray, *Structure*, 1994, **2**, 415–422.
37 P. K. Witting, A. G. Mauk and P. A. Lay, *Biochemistry*, 2002, **41**, 11495–11503.
38 H.-X. Liu, L.-Z. Li, B. He, S.-Q. Gao, G.-B. Wen and Y.-W. Lin, *Dalton Trans.*, 2018, **47**, 10847–10852.
39 P. Zhang, H. Yuan, J.-K. Xu, X.-J. Wang, S.-Q. Gao, X.-S. Tan and Y.-W. Lin, *ACS Catal.*, 2020, **10**, 891–896.
40 V. Yin, G. S. Shaw and L. Konermann, *J. Am. Chem. Soc.*, 2017, **139**, 15701–15709.